An explicit relation for the apparent phase velocity of Rayleigh waves in a vertically heterogeneous elastic half-space

Geophysical Journal International

Geophys. J. Int. (2014) **199,** 673–687
GJI Seismology

doi: 10.1093/gji/ggu283

An explicit relation for the apparent phase velocity of Rayleigh waves in a vertically heterogeneous elastic half-space

Carlo G. Lai,[1] Maria-Daphne Mangriotis[2] and Glenn J. Rix[3]

[1] *Department of Civil Engineering and Architecture, University of Pavia, Via Ferrata* 1, *I*-27100, *Pavia, Italy*
[2] *Institute of Petroleum Engineering, Heriot-Watt University, Edinburgh, EH*14 4*AS, United Kingdom. E-mail: mdmangriotis@gmail.com*
[3] *Geosyntec Consultants,* 2002 *Summit Blvd, Atlanta, GA* 30319, *USA*

Accepted 2014 July 21. Received 2014 July 18; in original form 2013 June 19

SUMMARY

This paper presents the mathematical derivation of an explicit relation for the apparent (or effective) phase velocity of Rayleigh waves in a vertically heterogeneous, isotropic elastic half-space for harmonic excitation. As a kinematical feature, the apparent phase velocity captures the superposition, in a spatial Fourier series, of the individual modes of propagation of Rayleigh waves and describes the speed of propagation of a composite waveform generated by a vertically oscillating point load. The relation, which is a function of the distance from the source, frequency and depth, depends explicitly on the modal phase and group velocities of Rayleigh waves, and their corresponding wavenumbers and eigenfunctions, which can be computed directly from the solution of the Rayleigh-wave eigenproblem. A practical scenario for the application of the notion of apparent Rayleigh-wave phase velocity is the modelling of the dispersion curve in the well-known surface wave measurement methods 'spectral analysis of surface waves' (SASW) and 'multichannel analysis of surface waves' (MASW). Apart from a theoretical motivation, the availability in surface wave testing of an explicit formula for the calculation of the apparent Rayleigh-wave phase velocity may lead to the development of a new class of inversion algorithms capable of taking into account the influence of all the modes of surface wave propagation. To demonstrate the exactness of the explicit relation, the predicted values of apparent phase velocity are compared to those computed synthetically from a numerical simulation of SASW and MASW testing for three case studies, which show both single as well as multiple mode dominance effects.

Key words: Surface waves and free oscillations.

1 INTRODUCTION

Since the prediction of surface Rayleigh waves by Lord Rayleigh (1887), their conditions of existence and propagation characteristics in elastic solids have been studied in great detail (e.g. Lamb 1904; Knopoff 1952; Achenbach 1984). In the context of seismology, in the 1950s and early 1960s researchers concentrated on the theoretical analysis of surface wave excitation and the existing relationship between group and phase velocities and elastic parameters of a crustal model (e.g. Ewing *et al.* 1957; Brune *et al.* 1961; Sato *et al.* 1962; Aslop 1963; Harkrider 1964; Haskell 1964). For a vertically heterogeneous, isotropic elastic half-space, several methods have been developed to solve the Rayleigh-wave eigenproblem (e.g. Gilbert & Backus 1966; Saito 1967; Takeuchi & Saito 1972; Wiggins 1976; Woodhouse 1980, 1988; Buland & Gilbert 1984). This requires determining modal wavenumbers (or alternatively the phase velocities) and eigenfunctions associated with a vertically heterogeneous half-space, knowing the elastic moduli (or equivalently the speeds of propagation of longitudinal *P* and transversal *S* waves), mass density and their variability with depth. The Rayleigh-wave eigenproblem is a forward problem. The inverse problem is that of computing the distribution with depth of one or more elastic moduli from the inversion of a set of experimentally measured dispersion functions. This inverse problem is the subject of geophysical prospecting and exploration seismology. A detailed review of the development of surface wave inversion algorithms in crustal-scale applications is presented by Romanowicz (2002).

The use of surface waves in engineering applications emerged in the 1950s with the Steady-State Rayleigh-wave Method (Jones 1958), followed by the SASW (spectral analysis of surface waves) technique introduced by Stokoe *et al.* (1994), the multistation methods commonly termed MASW (multichannel analysis of surface waves) explored by Lai & Rix (1998), Park *et al.* (1999) and Foti (2000), and more recently the refraction microtremor (ReMi) method developed by Louie (2001). All these aforementioned techniques exploit two important properties enjoyed by Rayleigh waves propagating in vertically heterogeneous half-spaces. These are 'geometric dispersion', which is the fact that their

speeds of propagation is frequency-dependant, and 'geometric attenuation', which is smaller in the direction of propagation if compared with that of corresponding *P* and *S* body waves.

Due to geometric dispersion, surface waves traveling in vertically heterogeneous half-spaces will not travel with a single phase and group velocity, but velocities which are a multivalued function of the frequency of excitation (Kennett 1983; Aki & Richards 2002). This phenomenon arises from a condition of constructing interference, within the heterogeneity of the medium, among rays that are either bent or reflected/refracted. Geometric dispersion is responsible for the existence of several modes of propagation, each traveling at a different phase and group velocity. For Rayleigh waves generated by harmonic sources, the various modes of propagation are superimposed in a spatial Fourier series. The corresponding phase velocity of the waveform, which is the result of interference among different modes, is termed in the literature 'apparent' or 'effective' Rayleigh-wave phase velocity. Tokimatsu *et al.* (1992) published a study on the effects of multiple modes of wave propagation in the dispersion characteristics of Rayleigh waves. In their paper, the authors provided a formal solution for the average apparent phase velocities (radial and vertical components), which is averaged over a range of offsets from a point source. Their analytical expressions involve the medium response, phase velocities and amplitude ratios between horizontal and vertical motions of each mode of propagation using the formulae obtained by Harkrider (1964) for the solution of the Rayleigh-wave eigenproblem, which was extended from the theory of Haskell (1953).

In this paper an exact, analytical relation for the apparent Rayleigh-wave phase velocity is derived, which is explicit in terms of fundamental quantities computed directly from the solution of the Rayleigh-wave eigenproblem. These fundamental quantities are the Rayleigh-wave wavenumbers (or alternatively the phase velocities) and eigenfunctions. The relation is of general validity in that it can be applied to any algorithm used to solve the Rayleigh-wave eigenproblem (e.g. matrix propagator method, thin layer method, numerical integration). The notion of apparent phase velocity leads naturally to the definition of a 'dispersion surface' that generalizes the concept of dispersion curve, which is valid for modal phase velocities. The dispersion surface reflects the dependence of the apparent phase velocity on the source characteristics, including the source type and orientation, its frequency, as well as the relative ratios of excitation amplitudes for different modes, and the source–receiver offset of. Thus, it is a 'local' quantity for it depends on the spatial position where it is measured.

The analytical relation derived in this paper is specific to a vertical point load on the free surface. The derivation assumes a far-field approximation, namely that the body waves generated by the vertically oscillating point load can be neglected. As suggested by Tokimatsu (1995), near-field effects are important up to a distance of $\frac{\lambda}{2}$ and 2λ for, respectively, normally dispersive half-spaces (i.e. media where the mechanical impedance increase monotonically with depth) and inversely dispersive half-spaces (i.e. media where the mechanical impedance varies irregularly with depth).

To demonstrate the exactness of the analytical expressions derived for computing the apparent Rayleigh-wave phase velocity, the apparent dispersion curves calculated with the proposed formulae are compared with those obtained from synthetic seismic data using SASW and MASW processing techniques. Three examples of normally as well as inversely dispersive media are illustrated. For normally dispersive media, the fundamental mode prevails in the vertical and horizontal motions. On the other hand, in inversely dispersive media like in the case of a stiff top layer overlying the half-space, higher modes are expected to dominate the response. The apparent phase velocity involves the contribution of single as well as multiple mode dominance with a relative modal weight, which, in general, changes with frequency.

Aside from a theoretical contribution, the explicit relation derived for computing the apparent phase velocity of Rayleigh waves may have a practical application in the solution of the Rayleigh-wave inverse problem. Traditionally, surface wave testing methods such as SASW and MASW techniques relied on the inversion of the fundamental mode, with only recent examples of inversions of single higher modes or a limited number of modes (Beaty 2000; Xia *et al.* 2000, 2003). An encouraging step on multimode inversion was presented by Ikeda *et al.* (2012) who compared observed phase velocities by the extended spatial autocorrelation method (ESPAC) to the effective phase velocities calculated using the Tokimatsu *et al.* (1992) formulae. In their study, the authors acknowledge the importance of having a theoretical solution for the (average) apparent phase velocity, which does not have aliasing constraints, and hence renders it continuous in the frequency range. On the other hand, Ikeda *et al.* (2012) suggest that inversion using apparent phase velocities may require prior information about the underlying half-space to obtain a better constrained shear wave velocity profile. A different approach, which extends to the full wavefield, is the inversion of expansion coefficients for recorded shallow-seismic wavefields presented by Forbriger (2003). In his procedure, which is robust even without *a priori* information, the entire full signal content is exploited including dispersion of higher modes, leaky modes and their true amplitudes. Last, but not least, Friederich (2003) proposed a waveform inversion scheme, which successfully takes into account mode coupling to infer the *S*-velocity structure using the multiple scattering theory of Friederich (1999).

The availability of our derived explicit, easy-to-implement formula to compute the Rayleigh-wave apparent phase velocity may help to develop algorithms for the measurement and the inversion of surface wave data, which take into account all the modes of propagation. Further efforts are needed on the experimental side for enhancing the ability of current methods of surface wave testing to measure the Raleigh apparent dispersion surface with a good degree of resolution.

2 APPARENT PHASE VELOCITY OF RAYLEIGH WAVES IN A VERTICALLY HETEROGENEOUS ISOTROPIC ELASTIC HALF-SPACE

It is well known (e.g. Aki & Richards 2002) that Rayleigh waves in vertically heterogeneous, isotropic, elastic half-spaces are dispersive and the main characteristics of wave motion are described by the Rayleigh-wave dispersion equation. The latter is nothing but a statement of

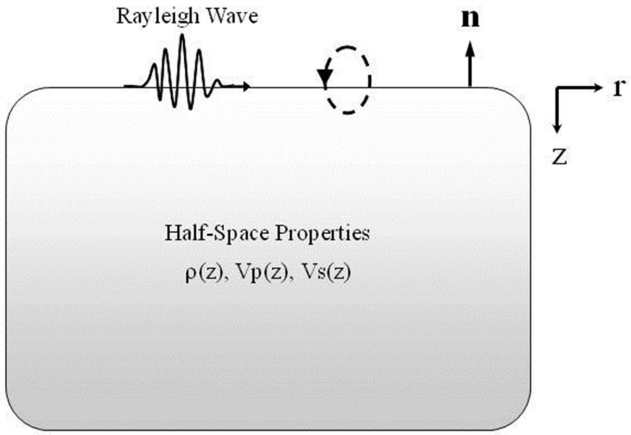

Figure 1. Material parameters and sign convention for the vertically heterogeneous, isotropic, elastic half-space.

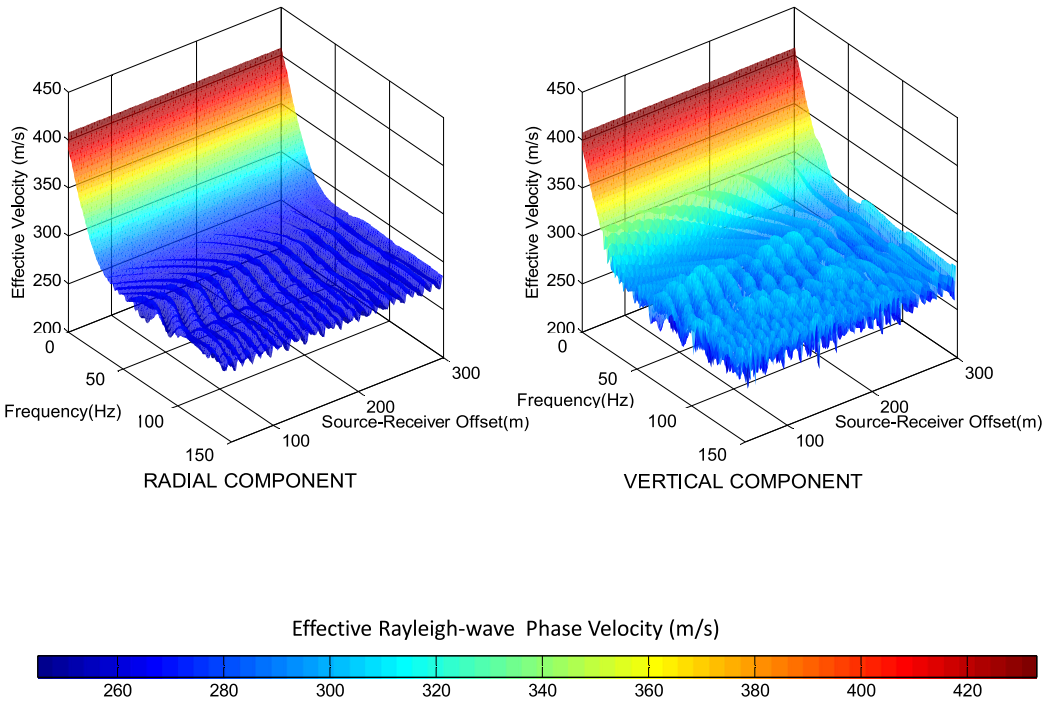

Figure 2. Example of dispersion surface showing the dependence of the effective Rayleigh-wave phase velocity with frequency and distance from the source. Geometry and medium parameters are defined in case study I of the applications.

the dependence of the speed of propagation of these waves upon frequency. In turn, the velocity of propagation is a multivalued function of frequency since in general at a given frequency different modes may co-exist.

If k is the wavenumber, ω the circular frequency and z the depth from the free surface (Fig. 1), the set $\{k_j(\omega), w_i(z,\ k_j, \omega)\}$ $(j = 1, M)$ defines a jth mode of propagation, and it is characterized by eigenvalues k_j and eigenfunctions $w_i(z,\ k_j, \omega)(i = 1, 4)$. The positive integer $M = M(\omega)$ represents the total number of modes associated with frequency ω, which may be finite or infinite depending on the z-dependence of the elastic moduli and mass density of the half-space and on the specific value of the excitation frequency. It can be shown that if the medium is composed of a finite number of homogeneous layers overlaying a homogeneous half-space, the total number of Rayleigh-wave modes is always finite (Ewing *et al.* 1957).

Rayleigh waves can be generated by mechanical sources applied at the boundary or in the interior of a half-space. If these sources are harmonic in time, the different modes of propagation are superimposed (Foti 2000). The phase velocity of the resulting waveform is the

Table 1. Case study I: medium parameters used for the validation of the explicit relation for the apparent Rayleigh-wave phase velocity. Parameters for case I are similar to those studied by Foti (2000).

Layer	Density (g cc^{-1})	V_p (m s^{-1})	V_s (m s^{-1})	Thickness (m)
1	1.8	600	300	5
2	1.8	700	400	10
3	1.8	800	450	∞

Table 2. Case study II: medium parameters used for the validation of the explicit relation for the apparent Rayleigh-wave phase velocity. Parameters for case II are similar to those studied by Foti (2000).

Layer	Density (g cc^{-1})	V_p (m s^{-1})	V_s (m s^{-1})	Thickness (m)
1	1.8	800	450	3
2	1.8	600	350	5
3	1.8	700	400	10
4	1.8	800	450	∞

'apparent' or 'effective' Rayleigh-wave phase velocity. In this section an explicit, analytical relation for the apparent Rayleigh-wave phase velocity is directly derived from the solution of the Rayleigh-wave eigenproblem.

In a vertically heterogeneous, isotropic elastic half-space, Rayleigh waves generated from point sources acting in a direction perpendicular to the boundary of the half-space propagate along cylindrical wave fronts (Ewing *et al.* 1957). It can be shown (Ben-Menahem & Singh 1981) that the wavefield originated by a harmonic vertical point source located at a position $r = 0,\ z = z_s$ can be expanded, in the radial direction, in a series of p-th order Hankel functions (p is an integer). For large values of r, the p-th order Hankel functions can be approximated by their asymptotic expansions involving complex exponentials. As a result, the particle displacement $u\,(r, z, \omega) = [u_r(r, z, \omega)e_r + u_z(r, z, \omega)e_z]$ resulting from the superposition of M distinct Rayleigh-wave modes can be written in cylindrical coordinates $\{r, z, \theta\}$ as follows (Aki & Richards 2002):

$$u_\beta(r, z, \omega) = \sum_{j=1}^{M} \left[A_\beta(r, z, \omega)\right]_j . \mathrm{e}^{\mathrm{i}(\omega t - k_j r + \phi_\beta)}, \tag{1}$$

where $\beta = r, z$ and $[A_\beta(r, z, \omega)]_j$ is the Rayleigh-wave displacement amplitude associated with the j-th mode of propagation. Finally, $\varphi_\beta = -\pi/4$ for $\beta = r$ and $\varphi_\beta = \pi/4$ for $\beta = z$. Eq. (1) shows, as expected, that $u_\beta(r, z, \omega)$ is independent from the azimuthal angle θ. The actual particle displacement is obtained by taking either the real or imaginary part of eq. (1). By choosing the latter, this equation becomes:

$$\Im\ \left[\mathrm{u}_\beta\ (r, z, \omega)\right] = \Im\ \left\{\sum_{j=1}^{M} \left[\mathrm{A}_\beta\ (r, z, \omega)\right]_j \mathrm{e}^{\mathrm{i}\ (\omega \cdot t - k_j \cdot r + \varphi_\beta)}\right\} = \sum_{j=1}^{M} \left[\left(\mathrm{C}_\beta\right)_j \sin\ (\omega t) - \left(\mathrm{D}_\beta\right)_j \cos\ (\omega t)\right], \tag{2}$$

where $(\mathrm{C}_\beta)_j = (\mathrm{A}_\beta)_j \cdot \cos\,(k_j \cdot r\ - \varphi_\beta)$ and $(D_\beta)_j = (\mathrm{A}_\beta)_j \cdot \sin\,(k_j \cdot r\ - \varphi_\beta)$. As shown in Appendix A, using simple trigonometric identities eq. (2) can be rewritten as follows:

$$\Im\ \left[\mathrm{u}_\beta\ (r, z, \omega)\right] =\ U_\beta\,(r, z, \omega) \cdot \sin\ \left[\omega t\ -\ \psi_\beta\,(r, z, \omega)\right], \tag{3}$$

where

$$U_\beta(r, z, \omega) = \left\{\sum_{i=1}^{M}\sum_{j=1}^{M} \left[A_\beta(r, z, \omega)\right]_i \left[A_\beta(r, z, \omega)\right]_j \cos\left[r(k_i - k_j)\right]\right\}^{0.5}, \tag{4}$$

$$\psi_\beta(r, z, \omega) = \tan^{-1}\left\{\frac{\sum_{i=1}^{M} \left[A_\beta(r, z, \omega)\right]_i \sin\,(k_i r + \varphi_\beta)}{\sum_{j=1}^{M} \left[A_\beta(r, z, \omega)\right]_j \cos\,(k_j r + \varphi_\beta)}\right\}. \tag{5}$$

Table 3. Case study III: medium parameters used for the validation of the explicit relation for the apparent Rayleigh-wave phase velocity.

Layer	Density (g cc^{-1})	V_p (m s^{-1})	V_s (m s^{-1})	Thickness (m)
1	1.8	400	200	5
2	1.8	200	100	10
3	1.8	600	300	15
4	1.8	800	400	∞

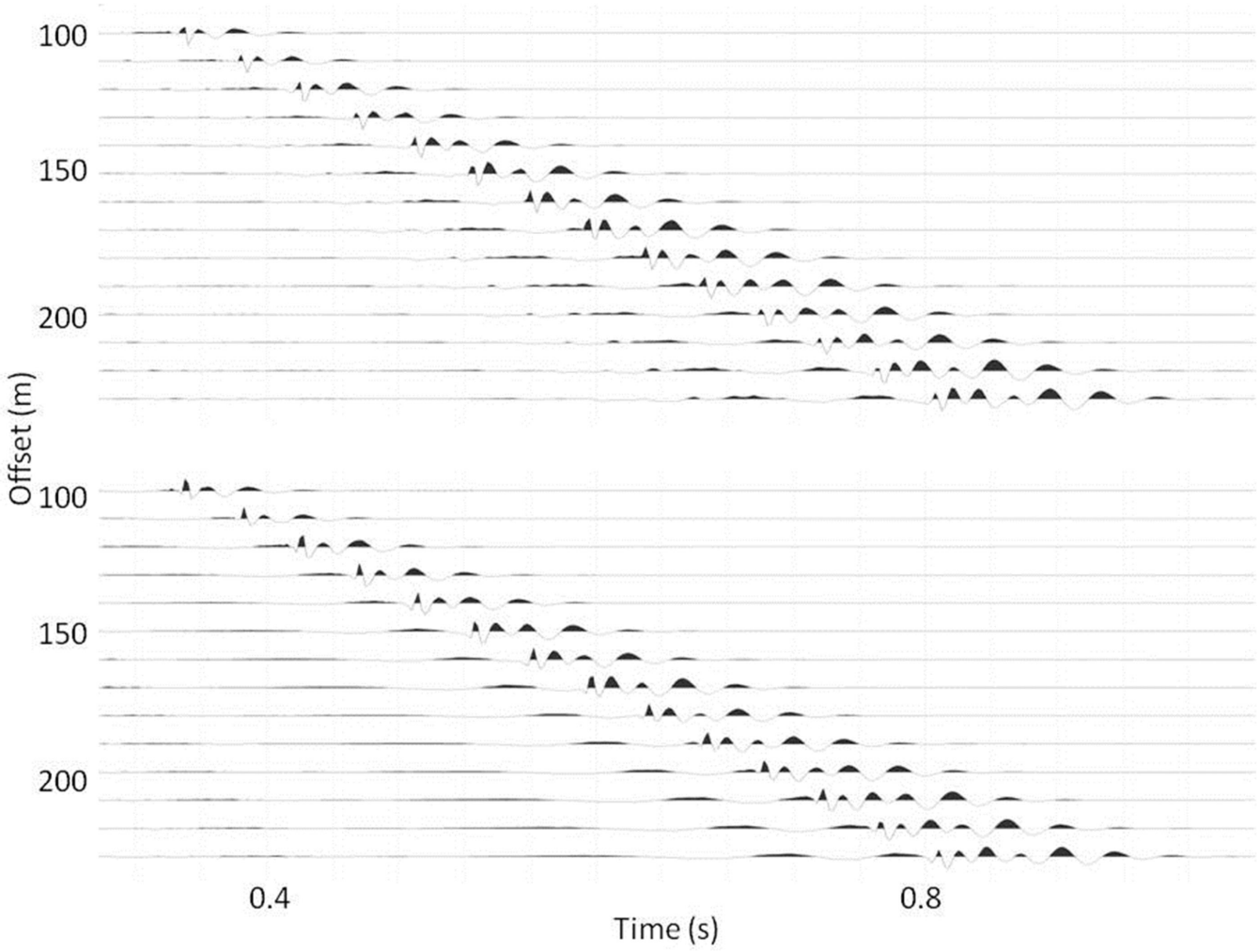

Figure 3. Case study I: synthetic shot gather for *z*-component (top panel) and *r*-component (bottom panel). Plotted for visual clarity are traces every 10 m offset.

From eq. (3), the expression:

$$\left[\omega t - \psi_\beta(r, z, \omega)\right] = \text{constant} \tag{6}$$

represents the equation of a wave front, since it is the locus of points having constant phase. Assuming the function $\psi_\beta(r, z, \omega)$ to be sufficiently smooth in r, eq. (6) can be differentiated with respect to time, to give:

$$\omega - \frac{\partial \psi_\beta(r, z, \omega)}{\partial r} \cdot \frac{\mathrm{d}r}{\mathrm{d}t} = 0, \tag{7}$$

which yields

$$\hat{V}_\beta(r, z, \omega) = \frac{\omega}{\left[\frac{\partial \psi_\beta(r, z, \omega)}{\partial r}\right]}, \tag{8}$$

where the symbol $\hat{V}_\beta(r, z, \omega)$ has been used to denote the 'apparent' or 'effective' Rayleigh-wave phase velocity.

It is evident from eq. (8) that the apparent Rayleigh-wave phase velocity is a local quantity, which means that its value depends on the spatial position where it is evaluated. At a fixed depth from the free surface $z = z_c$, the function $\hat{V}_\beta(r, z_c, \omega)$ describes a 'dispersion surface', that is, a 2-D surface showing the variation of the effective Rayleigh-wave phase velocity with frequency and distance from the source (Fig. 2).

Eq. (8) shows that different components of effective Rayleigh-wave phase velocity $\hat{V}_\beta(r, z, \omega)$ will, in general, travel at different phase velocities. Furthermore, since $\frac{\partial \hat{V}_\beta}{\partial t} = -\frac{\omega \cdot \hat{V}_\beta \frac{\partial \psi_\beta}{\partial r}}{\left[\frac{\partial \psi_\beta}{\partial r}\right]^2}$ is not, in general, equal to zero, the plane of constant phase accelerates (or decelerates) as it propagates along the free surface of the half-space.

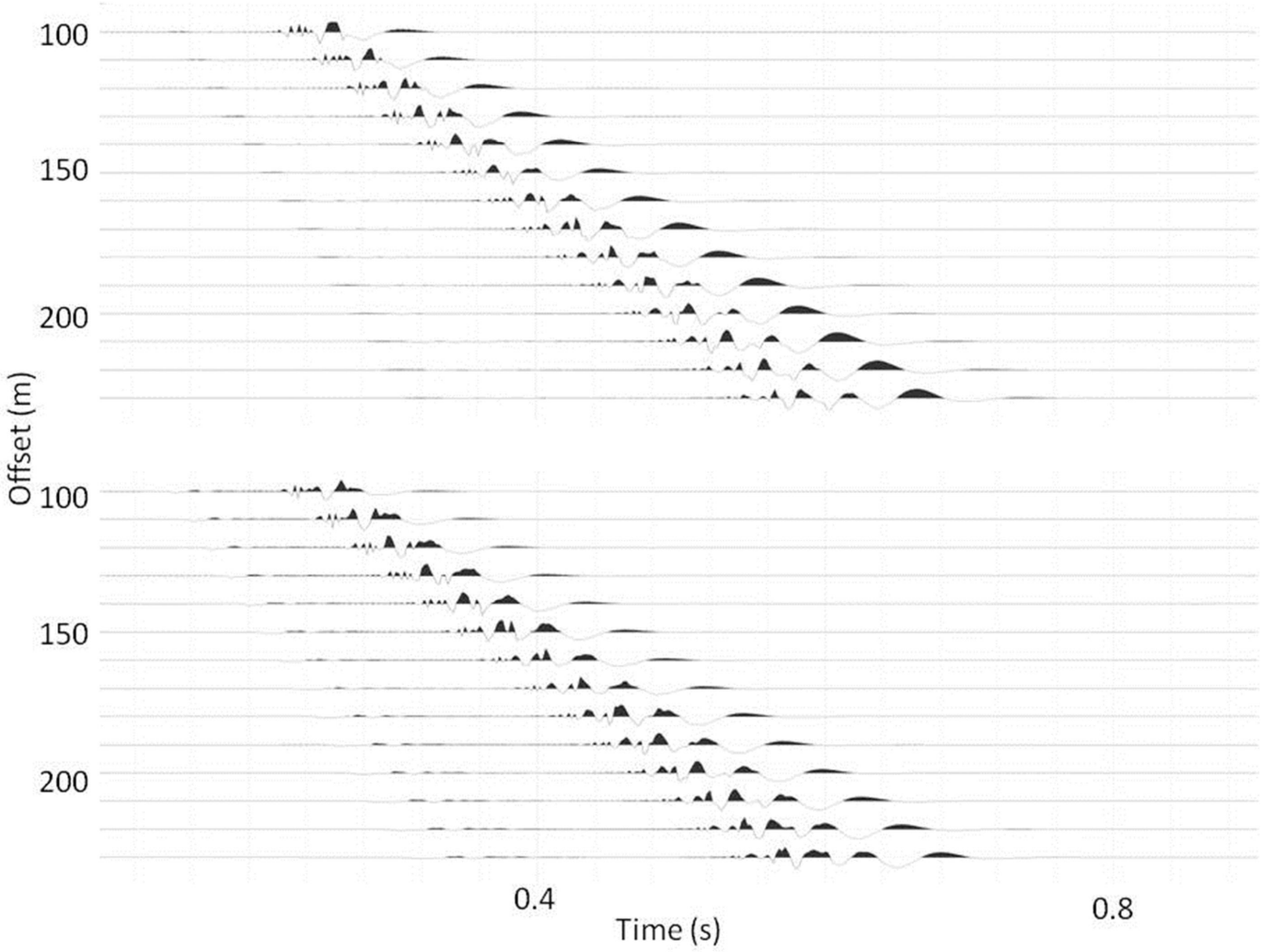

Figure 4. Case study II: synthetic shot gather for z-component (top panel) and r-component (bottom panel). Plotted for visual clarity are traces every 10 m offset.

In eq. (8), the term $\frac{\partial \psi_\beta}{\partial r}$ can be interpreted as an apparent Rayleigh-wave wavenumber and denoted as $\hat{k}_\beta(r, z, \omega)$. However, a decomposition of the argument of eq. (3) in the form $(\omega t - \hat{k}_\beta r)$, which is common for monochromatic waves, is no longer possible given that the apparent wavenumber $\frac{\partial \psi_\beta}{\partial r}$ being a local quantity, must be integrated over r to yield the phase $\psi_\beta(r, z, \omega)$.

Considering the definition of $\psi_\beta(r, z, \omega)$ given by eq. (5), it is possible to obtain from eq. (8), an explicit relation for the apparent Rayleigh-wave phase velocity. The result of the derivation, shown in Appendix B, is given by:

$$\hat{V}_\beta(r, z, \omega) = 2\omega \cdot \frac{\sum_{i=1}^{M}\sum_{j=1}^{M}\left\{(A_\beta)_i (A_\beta)_j \cos\left[r(k_i - k_j)\right]\right\}}{\sum_{i=1}^{M}\sum_{j=1}^{M}\left\{(A_\beta)_i (A_\beta)_j (k_i + k_j) \cos\left[r(k_i - k_j)\right]\right\}}. \tag{9}$$

For a harmonic point source $F_z e^{i\omega t}$ located at $r = 0,\ z = z_s$, the Rayleigh-wave displacement amplitudes $[A_\beta(r, z, \omega)]_j$ of the individual modes of propagation are related to the displacement eigenfunctions $w_1(z,\ k, \omega)$ and$w_2(z,\ k, \omega)$, and to other modal parameters by the following expression (Aki & Richards 2002):

$$\left[A_\beta(r, z, \omega)\right]_j = \begin{bmatrix} A_r(r, z, \omega) \\ A_z(r, z, \omega) \end{bmatrix}_j = \frac{F_z \cdot w_2(z_s,\ k_j, \omega)}{4 V_j U_j I_j \sqrt{2\pi r k_j}} \cdot \begin{bmatrix} w_1(z,\ k_j, \omega) \\ w_2(z,\ k_j, \omega) \end{bmatrix}, \tag{10}$$

where V_j, U_j and k_j are the phase, group velocity and wavenumber of the Rayleigh-wave j-th mode of propagation ($j = 1, M$), respectively. The term $I_j(z,\ k_j, \omega)$ is the first Rayleigh-wave energy integral associated with the j-th mode of propagation and is defined (Aki & Richards 2002) by

$$I_j(z,\ k_j, \omega) = \frac{1}{2}\int_0^\infty \rho(z)\left[w_1^2(z,\ k_j, \omega) + w_2^2(z,\ k_j, \omega)\right] \mathrm{d}z. \tag{11}$$

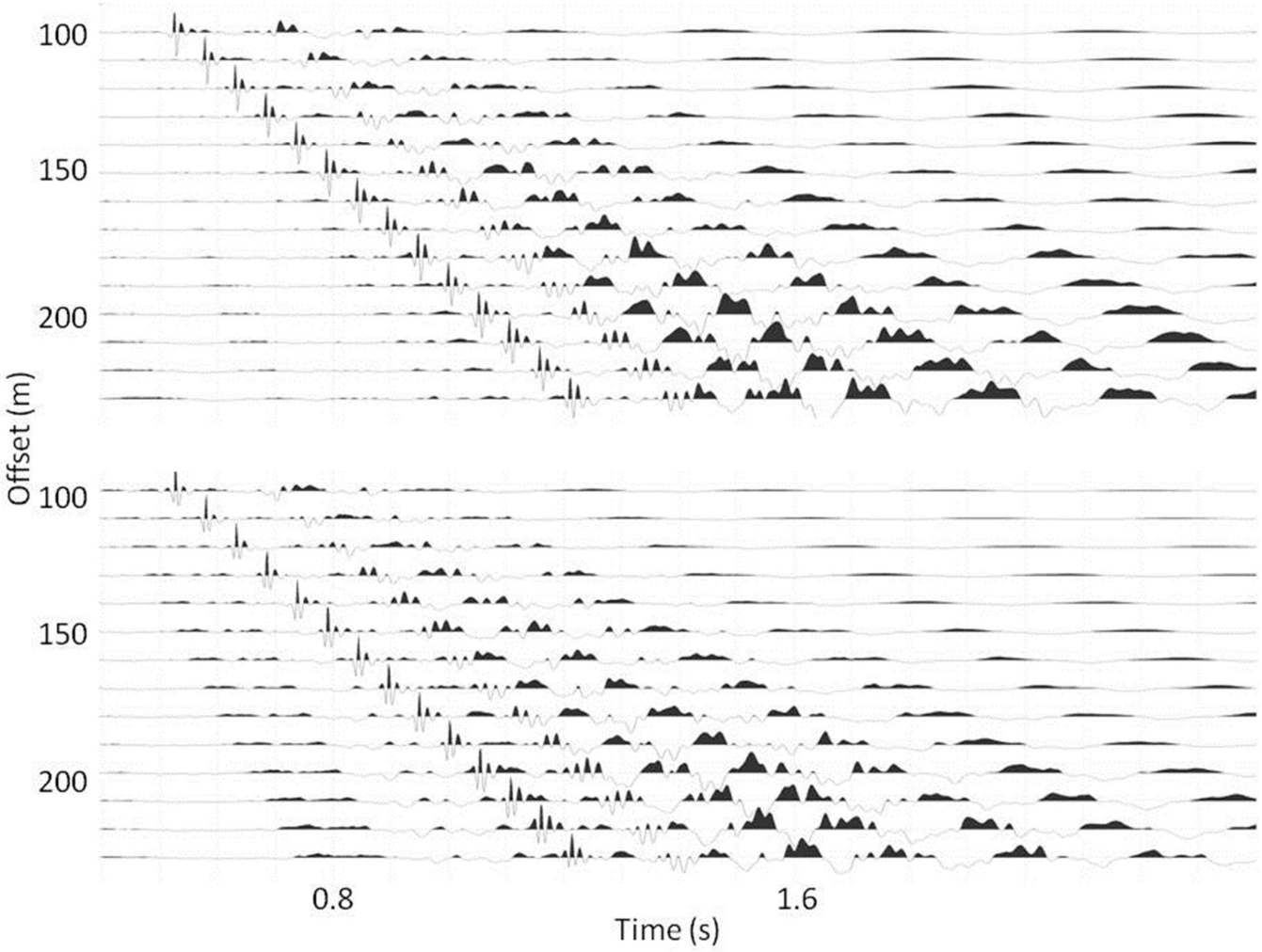

Figure 5. Case study III: synthetic shot gather for z-component (top panel) and r-component (bottom panel). Plotted for visual clarity are traces every 10 m offset.

By substituting eq. (10) into eq. (9), the expression for the apparent Rayleigh-wave phase velocity finally becomes

$$\hat{V}_r(r,z,\omega)=\frac{2\omega\sum_{i=1}^{M}\sum_{j=1}^{M}\left\{\frac{w_1(z,k_i)w_1(z,k_j)w_2(z_s,k_i)w_2(z_s,k_j)\cos\left[r(k_i-k_j)\right]}{(V_iU_iI_i)\left(V_jU_jI_j\right)\sqrt{k_ik_j}}\right\}}{\sum_{i=1}^{M}\sum_{j=1}^{M}\left\{\frac{w_1(z,k_i)w_1(z,k_j)w_2(z_s,k_i)w_2(z_s,k_j)(k_i+k_j)\cos\left[r(k_i-k_j)\right]}{(V_iU_iI_i)\left(V_jU_jI_j\right)\sqrt{k_ik_j}}\right\}}, \tag{12a}$$

$$\hat{V}_z(r,z,\omega)=\frac{2\omega\sum_{i=1}^{M}\sum_{j=1}^{M}\left\{\frac{w_2(z,k_i)w_2(z,k_j)w_2(z_s,k_i)w_2(z_s,k_j)\cos\left[r(k_i-k_j)\right]}{(V_iU_iI_i)\left(V_jU_jI_j\right)\sqrt{k_ik_j}}\right\}}{\sum_{i=1}^{M}\sum_{j=1}^{M}\left\{\frac{w_2(z,k_i)w_2(z,k_j)w_2(z_s,k_i)w_2(z_s,k_j)(k_i+k_j)\cos\left[r(k_i-k_j)\right]}{(V_iU_iI_i)\left(V_jU_jI_j\right)\sqrt{k_ik_j}}\right\}}, \tag{12b}$$

where $\hat{V}_r(r,z,\omega)$ and $\hat{V}_z(r,z,\omega)$ denote the components of the apparent Rayleigh-wave phase velocity along directions r and z, respectively. To reduce the length of the above expressions, the frequency dependence of the eigenfunctions $w_1(z,\ k,\omega)$ and $w_2(z,\ k,\omega)$ has been omitted.

As a final remark, it is noted from eqs (12a) and (12b) that the apparent Rayleigh-wave phase velocity is completely determined from the solution of the Rayleigh-wave eigenproblem and the nature (type, orientation and depth) of the source. In fact, recalling that $V_j=\frac{\omega}{k_j}$ and $U_j=\frac{\mathrm{d}\omega}{\mathrm{d}k_j}(j=1,M)$, all of the modal quantities appearing in eqs (12a) and (12b) can be calculated from the set $\{k_j,\ w_i(z,\ k_j,\omega)\}(i=1,4)$.

3 VALIDATION THROUGH NUMERICAL MODELLING

The explicit relations derived in the previous section for the apparent Rayleigh-wave phase velocity are hereby validated by comparing the predictions of eqs (12a) and (12b) with the dispersion curves computed using synthetic surface wave data generated from a simulation of

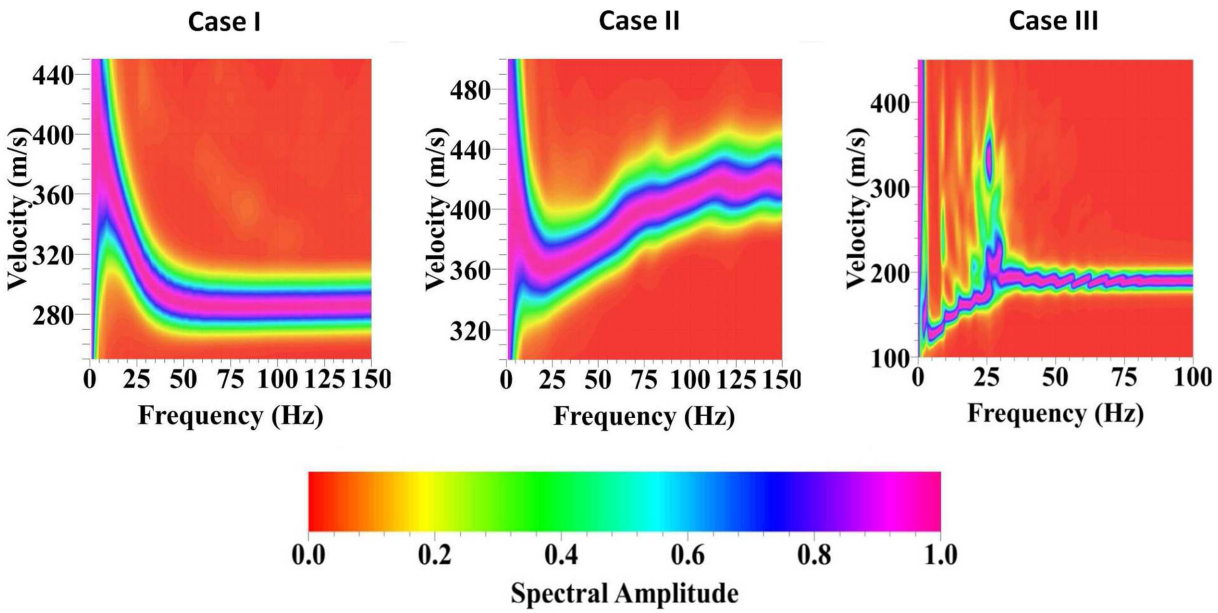

Figure 6. Rayleigh-wave phase velocity spectra computed from *f–k* analysis of MASW synthetic data for case studies I, II and III. Note that for case III, multiple modes dominate, which results in multiple Rayleigh-wave phase velocity for each individual frequency in the frequency range of ∼20–35 Hz.

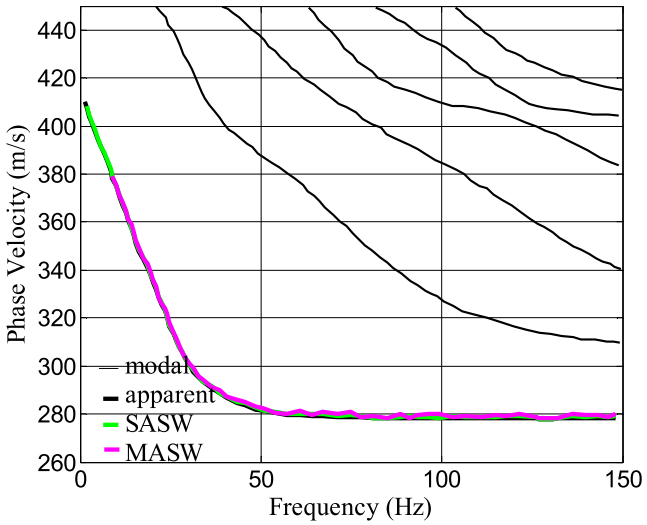

Figure 7. Case study I: comparison of phase velocity dispersion curves showing (i) modal phase velocities, (ii) effective phase velocity, and phase velocity computed from synthetic data using (iii) SASW and (iv) MASW methods.

SASW and MASW testing configuration. The comparison has been carried out for both the radial and the vertical components (r and z) of motion. In what follows, the procedure adopted to construct the apparent dispersion curves from synthetic surface wave data will be briefly reviewed.

When using harmonic sources, the SASW method yields an apparent dispersion curve since the generated wavefield is made up of the superposition of all the modes of propagation. Thus in the two-station SASW configuration, the measured Rayleigh-wave speed of propagation is the apparent and not the modal phase velocity. On the other hand, the MASW array configuration should yield in principle, well-separated modal dispersion curves. However, in many practical applications of MASW testing, it may not be possible to separate all the modes due, for instance, to a limited array length, inadequate interreceiver spacing, the presence of leaky waves, near-field effects and existence of osculation points.

Another important issue related to SASW and MASW testing configurations concerns the relative amplitudes of the different modes of propagation. If only one mode dominates the wavefield at a specific frequency, then the phase difference computed from the two-station SASW method varies smoothly with the distance from the source. This will yield a relatively constant estimate of phase velocity, regardless of the position of the receiver pairs. Similarly, in MASW testing, when a single mode dominates, the *f–k* spectrum will provide a single dominant value of phase velocity at that frequency. If, however, multiple modes have similar amplitudes, spatial beating effects may occur.

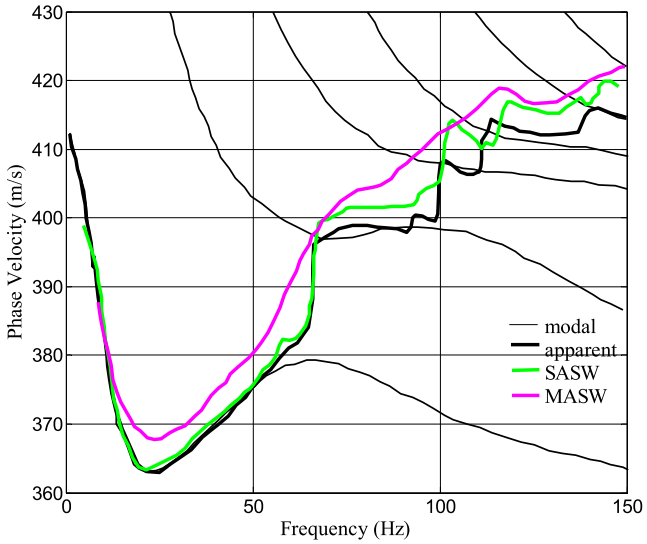

Figure 8. Case study II: comparison of phase velocity dispersion curves showing (i) modal phase velocities, (ii) effective phase velocity, and phase velocity computed from synthetic data using (iii) SASW and (iv) MASW methods.

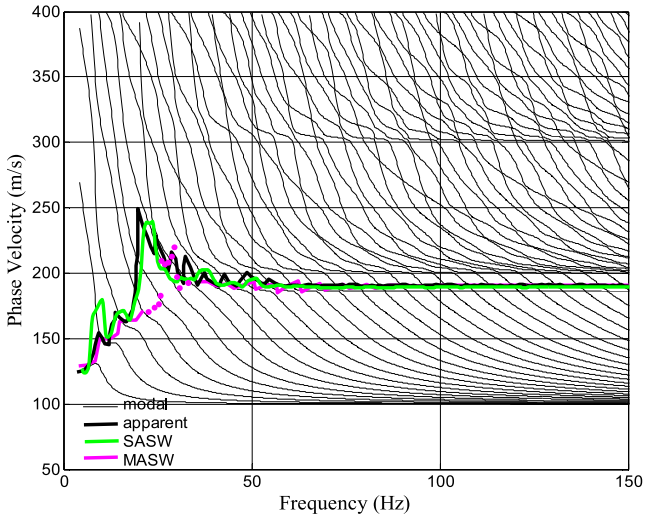

Figure 9. Case study III: comparison of phase velocity dispersion curves showing (i) modal phase velocities, (ii) effective phase velocity, and phase velocity computed from synthetic data using (iii) SASW and (iv) MASW methods. Please note that in the frequency range ∼20–35 Hz, picking of the dispersion curve for MASW is not straightforward (part of dispersion curve shown as dots as opposed to a line), if not ambivalent, given that multiple modes have similar magnitudes, as was also seen in Fig. 6.

This will cause the phase velocity measured with SASW configuration to vary significantly with receiver offset, whereas in MASW testing multiple values of phase velocity are obtained (e.g. Foti 2000; Forbriger 2003; Strobbia & Foti 2006; Ikeda *et al.* 2012).

To compare the apparent Rayleigh-wave phase velocity computed from eqs (12a) and (12b) with the dispersion curves derived from SASW and MASW testing configurations, three case studies are considered. The first is that of a normally dispersive half-space, where the mechanical impedance increases regularly with depth. The other two cases, have a stiff top layer with lower velocity zones existing at intermediate depths (Tables 1–3). Due to the local nature of the apparent phase velocity, the construction of the apparent dispersion curve from eqs (12a) and (12b) was carried out by using the heuristic approach of eliminating the dependence of these equations on the distance from the source by averaging the apparent phase velocity over the length of the receiver array, which was adopted in the simulations of MASW and SASW testing configurations.

Synthetic seismograms were computed with the wavenumber integration method using the 'Computer Programs in Seismology' (http://www.eas.slu.edu/eqc/eqc_cps/CPS/CPS330/) written by R.B. Herrmann (1994). Since the explicit relations obtained for the apparent Rayleigh-wave phase velocity do not account for body waves, synthetic traces with source–receiver offsets larger than 100 m are considered, which is well above the 2λ limit set to avoid near-field effects in inversely dispersive half-spaces and the $\lambda/2$ limit for normally dispersive media (Holzlohner 1980; Herrmann 1994; Tokimatsu 1995). The model receiver spacing was set equal to 1 m, and the maximum source–receiver distance at 256 m, yielding a total of 157 synthetic traces. Total record length was set to 4 s, and sampling rate to 2 ms. Figs 3 to 5 show the synthetic shot gathers of vertical and horizontal components of particle velocity for the three case studies considered.

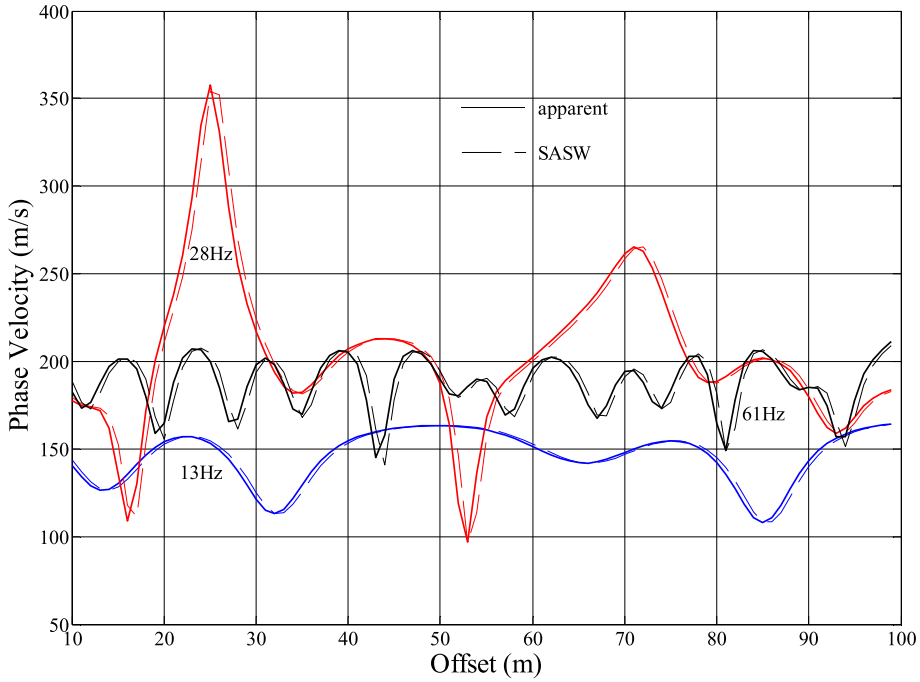

Figure 10. Comparison of apparent phase velocity as a function of offset using the explicit formula (eq. 12b), and SASW method. Three frequencies are selected for display: 13 Hz (blue), 28 Hz (red) and 61 Hz (black).

Using the SASW and MASW methodologies, we constructed synthetic dispersion curves using a frequency step of 0.2 Hz and frequency bandwidth from 5 to 150 Hz. In the case of SASW technique, the phase differences between 155 receiver pairs are calculated with an interreceiver distance of 2 m. In this way the synthetic Rayleigh-wave phase velocity was computed at 1 m intervals. For SASW testing configuration, the mean of the individual experimental phase velocities was taken over the entire model array to simulate the measurement of an experimental apparent Rayleigh-wave phase velocity. To analyse the synthetic data with the MASW technique, the computer program GEOPSY (Wathelet 2008; http://www.geopsy.org/) has been used to calculate the *f–k* spectrum for each case study using the complete set of traces (157 traces).

Fig. 6 shows the vertical component of the velocity spectra for the three case studies derived from the *f–k* transform of the MASW array configuration. The dispersion curve from the *f–k* spectra was computed as the average value between a lower and upper envelope around the *f–k* spectra peaks (recommendation by C. Cornou, personal communication, 2010). Equivalent results were obtained from the horizontal component of the synthetic data. Note that for the third case study, multiple modes have similar spectral amplitudes in the frequency range ∼ 20–35 Hz resulting in multiple values of phase velocity.

Figs 7 to 9 show for the three case studies the apparent dispersion curves computed from SASW and MASW synthetic data, along with the effective dispersion curve calculated using eqs (12a) and (12b) and denoted ‘apparent’ in the figures. The agreement between SASW and MASW curves and the ‘apparent’ dispersion curve is good for all the three case studies. A perfect match among the curves would have been unattainable due to significantly different procedures adopted to construct the three types of apparent dispersion curves. In addition to the apparent Rayleigh-wave phase velocity, also plotted are the modal phase velocities, computed with the computer code ‘Hisalai’ written by C.G. Lai in 1997, a modification of computer code created by Y. Hisada (1994, 1995). As expected for case study I, which is a normally dispersive soil profile, the contribution to the apparent phase velocity is primarily from the fundamental mode. On the other hand, for cases II and III contributions from higher modes become significant. This implies that an inversion process, which does not take into account higher modes when their contribution is important, may yield unreliable results. A sensible remedy would be to invert the measured dispersion curve for the apparent and not the modal Rayleigh-wave phase velocity.

The results plotted in Figs 7 to 9 are for the vertical component of wave motion. Similar processing was performed for the radial component, which, however, yielded essentially identical results. For the idealized situation (i.e. ‘perfect’ source and receiver orientation and absence of background noise) the vertical and radial components of wave motion will in general be different in terms of the computed seismograms (Figs 3 to 5). On the other hand, the apparent phase velocity (both theoretical from eqs 12a and 12b as well as that computed from synthetic traces) turn out to be equivalent for the two components. This result is consistent with the expectation that the average information carried by the two components of ground motion should be the same, in the sense that they both reflect the signature of the specific characteristics of a half-space (i.e. the number and thicknesses of the layers, the elastic moduli and the mass density variation with depth). In real physical experiments, however, it is expected that the theoretical formula for the apparent Rayleigh-wave phase velocity will be best validated with the vertical components of the experimental array, given that they isolate the Rayleigh wave, and that they typically have higher signal-to-noise ratio for vertically oriented sources.

Fig. 10 shows the monochromatic computation of the apparent phase velocity as a function of offset from the source, using eq. (12b), for the medium properties of case III, at three selected frequencies: 13, 28 and 61 Hz. The apparent phase velocity fluctuates as a function of distance from the source, and is averaged to a single value, as displayed Fig. 9. For comparison, the SASW-derived phase velocities are also plotted for receiver pairs, one located at the offset and the other at the offset plus 1 m. From Fig. 10 we see good agreement between our derived formula for the apparent phase velocity and that derived from SASW, however, further testing, both numerical and in the field, is required to assess the practicality of using the SASW configuration for inversion of apparent phase velocity. Finally, for the numerical validation, a rather ideal configuration of the synthetic array has been chosen, both in terms of receiver spacing as well as receiver array length, merely to confirm the predictions for the explicit relation with the results from SASW and MASW methods. A complete analysis of the parameters used for SASW and MASW computation of apparent phase velocity is outside the scope of this paper.

4 CONCLUDING REMARKS

This paper illustrated the mathematical derivation of an explicit, analytical relation for the apparent phase velocity of Rayleigh waves propagating in a vertically heterogeneous, isotropic, elastic half-space and generated by an oscillating, vertical point source applied at the free surface of the ground. The derivation assumes that the wavefield is only composed of surface Rayleigh waves and thus it is valid in the far-field approximation where the contribution of the body waves can be neglected. The relation has been obtained for both the vertical and radial component of ground motion. Its practical implementation only requires knowledge of the modal wavenumbers (or alternatively the phase velocities) and eigenfunctions, which constitute the solution of the Rayleigh-wave eigenproblem. Thus, its applicability is general and independent of the particular algorithm used to calculate wavenumbers and eigenfunctions.

In a layered half-space, the apparent phase velocity results from the superposition of a finite number of modes of propagation of Rayleigh waves, each traveling at a different phase velocity. It is a local quantity in the sense that, at a given frequency, its value varies continuously with distance from source. The validation of the formulae to compute the apparent Rayleigh-wave phase velocity was carried out through a series of numerical simulations of surface wave testing using both SASW and MASW array configurations. The analysis was performed for three case studies corresponding to both normally dispersive and inversely dispersive soil profiles. The explicit relation for the apparent phase velocity matches well the dispersion curves calculated from synthetic SASW and MASW surface wave data, thereby confirming the correctness of the relation.

ACKNOWLEDGEMENTS

Some of the mathematical derivations presented in this paper are borrowed from the PhD dissertation of C.G. Lai, Chapter 3, listed in the references as Lai & Rix (1998). This material was based upon work supported by the National Science Foundation under Grant No. CMS-9402358 and the U.S. Geological Survey under Award No. 1434-95-G-2634. Any opinions, findings and conclusions or recommendations expressed in this material are those of the authors and do not necessarily reflect the views of the National Science Foundation and the U.S. Geological Survey. The authors are grateful to Dr Clifford J. Astill of the National Science Foundation and Dr John D. Sims of the U.S. Geological Survey for their support and encouragement. The authors would also like to thank Dr Friederich, Dr Diasakos and two anonymous reviewers for their insightful comments which improved the quality of the manuscript.

REFERENCES

Achenbach, J.D., 1984. *Wave Propagation in Elastic Solids,* North-Holland.

Aki, K. & Richards, P.G., 2002. *Quantitative Seismology,* University Science Books.

Aslop, L.E., 1963. Free spheroidal vibrations of the Earth, *Bull. seism. Soc. Am.,* **53,** 483–502.

Beaty, K.S., 2000. Determination of near-surface variability using Rayleigh-waves, *MSc thesis,* University of Alberta, Alberta.

Ben-Menahem, A. & Singh, S.J., 1981. *Seismic Waves and Sources,* Springer-Verlag.

Brune, J.W., Nafe, J.E. & Alsop, L.E., 1961. The polar phase shift of surface waves on a sphere, *Bull. seism. Soc. Am.* **51,** 247–257.

Buland, R.P. & Gilbert, F., 1984. Computation of free oscillations of the Earth, *J. Comput. Phys.,* **54,** 95–114.

Ewing, W.M., Jardetzky, W.S. & Press, F., 1957. *Elastic Waves in Layered Media,* ed. Shrock, R., McGraw-Hill.

Forbriger, T., 2003. Inversion of shallow-seismic wavefields. Part 1: wavefield transformation, *Geophys. J. Int.,* **153,** 719–734.

Foti, S., 2000. Multi-station methods for geotechnical characterisation using surface waves, *PhD thesis,* Politecnico di Torino, Torino.

Friederich, W., 1999. Propagation of seismic shear and surface waves in a laterally heterogeneous mantle by multiple forward scattering, *Geophys. J. Int.,* **136,** 180–204.

Friederich, W., 2003. The S-velocity structure of the East Asian mantle from the inversion of shear and surface waveforms, *Geophys. J. Int.,* **153,** 88–102.

Gilbert, F. & Backus, G.E., 1966. Propagator matrices in elastic wave and vibration problem, *Geophysics,* **31,** 326–333.

Harkrider, D.G., 1964. Surface waves in multi-layered elastic media. 1, Rayleigh and Love waves from buried sources in a multilayered elastic half-space, *Bull. seism. Soc. Am.,* **54,** 627–680.

Haskell, B., 1953. The dispersion of surface waves on multilayered media, *Bull. seism. Soc. Am.,* **43,** 17–34.

Haskell, B., 1964. Radiation pattern of surface waves from point sources in a multi-layered medium, *Bull. seism. Soc. Am.,* **54,** 377–393.

Herrmann, P.B., 1994. *Computer Programs in Seismology,* User's Manual, Vol. II, St. Louis University.

Hisada, Y., 1994. An efficient method for computing green's functions for a layered half-space with sources and receivers at close depths, *Bull. seism. Soc. Am.,* **84,** 1456–1472.

Hisada, Y., 1995. An efficient method for computing green's functions for a layered half-space with sources and receivers at close depths (Part 2), *Bull. seism. Soc. Am.,* **85,** 1080–1093.

Holzlohner, U., 1980. Vibrations of the elastic half-space due to vertical surface loads, *Earthq. Eng. Struct. Dyn.*, **8,** 405–414.

Ikeda, T., Matsuoka, T., Tsuji, T. & Hayashi, K., 2012. Multimode inversion with amplitude response of surface waves in the spatial autocorrelation method, *Geophys. J. Int*., **190,** 541–552.

Jones, J.B., 1958. In-situ measurements of the dynamic properties of soil by vibration method, *Geotechnique,* **8,** 1–21.

Kennett, B.L.N., 1983. *Seismic Wave Propagation in Stratified Media,* Cambridge Univ. Press.

Knopoff, L., 1952. On Rayleigh-wave velocities, *Bull. seism. Soc. Am.,* **42,** 307–308.

Lai, C.G. & Rix, G.J., 1998. *Simultaneous inversion of Rayleigh phase velocity and attenuation for near-surface site characterization,* Rep No. GIT-CEE/GEO-98-2, School of Civil and Environmental Engineering, Georgia Institute of Technology, Georgia.

Lamb, H., 1904. On the propagation of tremors over the surface of an elastic solid, *Phil. Trans. R. Soc. Lond.,* **203,** 1–42.

Louie, J.N., 2001. Faster, Better: Shear wave velocity to 100 meters depth from refraction microtremor analysis, *Bull. seism. Soc. Am.,* **91,** 347–364.

Park, C.B., Miller, R.D. & Xia, J., 1999. Multichannel analysis of surface waves, *Geophysics,* **64,** 800–808.

Rayleigh, J.W.S., 1887. On waves propagating along the plane surface of an elastic solid, *Proc. Lond. Math. Soc.,* **s1–17**(1), 4–11.

Romanowicz, B., 2002. Inversion of surface waves: a review, in *Handbook of Earthquake and Engineering Seismology,* Chap. 11, pp. 141–173, ed. Lee, W.H.K., Academic Press.

Saito, M., 1967. Excitation of free oscillations and surface waves by a point source in a vertically heterogeneous Earth, *J. geophys. Res.,* **72,** 3689–3699.

Sato, Y., Usami, T. & Ewing, M., 1962. Basic study of the oscillation of a homogeneous elastic sphere, *Geophys. Mag.,* **31,** 237–242.

Stokoe, K.H., Wright, S.G., Bay, J. & Roesset, J.M., 1994. Characterization of Geotechnical Sites by SASW Method, in *Geophysical Characterization of Sites,* pp. 15–25, ed. Woods, R.D., Oxford & IBH Publ.

Strobbia, C. & Foti, S., 2006. Multi-offset phase analysis of surface wave data (MOPA), *J. appl. Geophys.,* **59,** 300–313.

Takeuchi, M. & Saito, M., 1972. Seismic surface waves, seismology: surface waves and free oscillations, in *Methods in Computational Physics,* **Vol. 11,** pp. 217–295, ed. Bolt, B.A., Academic Press.

Tokimatsu, K., 1995. Geotechnical site characterization using surface waves, in *Proceedings of First International Conference on Earthquake Geotechnical Engineering,* IS-Tokyo '95, pp. 1333–1368.

Tokimatsu, K., Tamura, S. & Kojima, H., 1992. Effects of multiple modes on rayleigh-wave dispersion characteristics, *J. Geotech. Eng.,* ASCE, **118,** 1529–1543.

Wathelet, M., 2008. An improved neighborhood algorithm: parameter conditions and dynamic scaling, *Geophys. Res. Lett.,* **35,** L09301, doi:10.1029/2008GL033256.

Wiggins, R., 1976. A fast new computational algorithm for free oscillations and surface waves, *Geophys. J. R. astr. Soc.,* **47,** 135–150.

Woodhouse, J.H., 1980. Efficient and stable methods for performing seismic calculations in stratified media, *physics of the earth's interior,* in *Proceedings of International School of Physics 'Enrico Fermi', Course 78*, pp. 127–151, Dziewonski, A.M. & Boschi, E., North-Holland Pub. Co., Amsterdam.

Woodhouse, J.H., 1988. The calculation of eigenfrequencies and eigenfunctions of the free oscillations of the Earth and the Sun, in *Seismological Algorithms,* pp. 321–370, ed. Doornbos, D.J., Academic Press.

Xia, J., Miller, R.D. & Park, C.D., 2000. Advantages of calculating shear-wave velocity from surface waves with higher modes, in *Proceedings of 70th Annual International Meeting SEG,* Expanded Abstracts, pp. 1295–1298.

Xia, J., Miller, R.D., Park, C.D. & Tian, G., 2003. Inversion of high frequency surface waves with fundamental and higher modes, *J. appl. Geophys.,* **52,** 45–57.

APPENDIX A

Starting from eq. (2):

$$\Im\left[\mathrm{u}_\beta\ (r,z,\omega)\right] = \Im\left\{\sum_{j=1}^{M}\left[\mathrm{A}_\beta\,(r,z,\omega)\right]_j \mathrm{e}^{\mathrm{i}\,(\omega\cdot t - k_j\cdot r + \varphi_\beta)}\right\} = \sum_{j=1}^{M}\left[\left(\mathrm{C}_\beta\right)_j \sin(\omega t) - \left(\mathrm{D}_\beta\right)_j \cos(\omega t)\right]. \tag{A1}$$

This equation can be rewritten as

$$\Im\left[\mathrm{u}_\beta\ (r,z,\omega)\right] = U_\beta\,(r,z,\omega)\cdot\sin\left[\omega t - \psi_\beta\,(r,z,\omega)\right] \tag{A2}$$

with

$$U_\beta\,(r,z,\omega) = \sqrt{\left(\sum_{i=1}^{M}\left[A_\beta(r,z,\omega)\right]_i\cdot\cos(k_i r+\varphi_\beta)\right)^2 + \left(\sum_{i=1}^{M}\left[A_\beta(r,z,\omega)\right]_i\cdot\sin(k_i r+\varphi_\beta)\right)^2} \tag{A3}$$

and

$$\psi_\beta(r,z,\omega) = \tan^{-1}\left\{\frac{\sum_{i=1}^{M}\left[A_\beta(r,z,\omega)\right]_i\cdot\sin(k_i r+\varphi_\beta)}{\sum_{i=1}^{M}\left[A_\beta(r,z,\omega)\right]_i\cdot\cos(k_i r+\varphi_\beta)}\right\}. \tag{A4}$$

Using simple algebra, the argument of the square-root term of eq. (A3) can be rewritten as

$$\left(\sum_{i=1}^{M}\left[A_\beta\,(r,z,\omega)\right]_i\cdot\cos(k_i r+\varphi_\beta)\right)^2 + \left(\sum_{i=1}^{M}\left[A_\beta\,(r,z,\omega)\right]_i\cdot\sin(k_i r+\varphi_\beta)\right)^2$$

$$= \sum_{i=1}^{M}\sum_{j=1}^{M}\left[A_\beta(r,z,\omega)\right]_i\cdot\left[A_\beta(r,z,\omega)\right]_j\cdot\cos\left[r(k_i-k_j)\right]. \tag{A5}$$

Assuming eq. (A5) to be true for $M = n$, it suffices to prove that it is also true for $n + 1$:

$$\left(\sum_{i=1}^{n+1}[A_i\cos(\nu_i)]\right)^2+\left(\sum_{i=1}^{n+1}[A_i\sin(\nu_i)]\right)^2=\left(\sum_{i=1}^{n}[A_i\cos(\nu_i)]\right)^2+(A_{n+1})^2\cos^2(\nu_{n+1})$$
$$+2A_{n+1}\left(\sum_{i=1}^{n}[A_i\cos(\nu_i)]\right)\cos(\nu_{n+1})$$
$$+\left(\sum_{i=1}^{n}[A_i\sin(\nu_i)]\right)^2+(A_{n+1})^2\sin^2(\nu_{n+1})$$
$$+2A_{n+1}\left(\sum_{i=1}^{n}[A_i\sin(\nu_i)]\right)\sin(\nu_{n+1}). \tag{A6}$$

In eq. (A6) for ease of notation, the subscript β has been dropped and the term $k_i r + \varphi_\beta$ has been replaced by the ν_i term. Eq. (A6) can be written as

$$\sum_{i=1}^{n}\sum_{j=1}^{n}\left[A_iA_j\right]\cos\left[\nu_i-\nu_j\right]+(A_{n+1})^2+2A_{n+1}\left[\sum_{i=1}^{n}A_i\cos(\nu_i)\cos(\nu_{n+1})+\sum_{i=1}^{n}A_i\sin(\nu_i)\sin(\nu_{n+1})\right], \tag{A7}$$

which using simple trigonometry can be rewritten as

$$\sum_{i=1}^{n}\sum_{j=1}^{n}\left[A_iA_j\right]\cos\left[\nu_i-\nu_j\right]+(A_{n+1})^2\cos(\nu_{n+1}-\nu_{n+1})+2A_{n+1}\left[\sum_{i=1}^{n}A_i\cos(\nu_i-\nu_{n+1})\right]=\sum_{i=1}^{n+1}\sum_{j=1}^{n+1}\left[A_iA_j\right]\cos\left[\nu_i-\nu_j\right]. \tag{A8}$$

APPENDIX B

Starting from eq. (8), namely

$$\hat{V}_\beta(r,z,\omega)=\frac{\omega}{\left[\frac{\partial\psi_\beta(r,z,\omega)}{\partial r}\right]}. \tag{B1}$$

Given the definition of ψ_β as:

$$\psi_\beta(r,z,\omega)=\tan^{-1}\left\{\frac{\sum_{i=1}^{M}\left[A_\beta(r,z,\omega)\right]_i\cdot\sin(k_ir+\varphi_\beta)}{\sum_{j=1}^{M}\left[A_\beta(r,z,\omega)\right]_j\cdot\cos(k_jr+\varphi_\beta)}\right\}, \tag{B2}$$

and differentiating with respect to r, yields

$$\frac{\partial\psi_\beta}{\partial r}=\left[\frac{\Xi+\Psi}{1+\left[\frac{\sum_{i=1}^{M}\left[A_{\beta i}\sin(k_ir+\varphi_\beta)\right]}{\sum_{i=1}^{M}\left[A_{\beta i}\cos(k_ir+\varphi_\beta)\right]}\right]^2}\right], \tag{B3}$$

where

$$\Xi=\left[\frac{\sum_{i=1}^{M}A_{\beta i}k_i\cos(k_ir+\varphi_\beta)\sum_{i=1}^{M}A_{\beta i}\cos(k_ir+\varphi_\beta)+\sum_{i=1}^{M}A_{\beta i}k_i\sin(k_ir+\varphi_\beta)\sum_{i=1}^{M}A_{\beta i}\sin(k_ir+\varphi_\beta)}{\left(\sum_{i=1}^{M}\left[A_{\beta i}\cos(k_ir+\varphi_\beta)\right]\right)^2}\right]$$

and

$$\Psi=\left[\frac{\sum_{i=1}^{M}\frac{\partial A_{\beta i}}{\partial r}\sin(k_ir+\varphi_\beta)\sum_{i=1}^{M}A_{\beta i}\cos(k_ir+\varphi_\beta)-\sum_{i=1}^{M}\frac{\partial A_{\beta i}}{\partial r}\cos(k_ir+\varphi_\beta)\sum_{i=1}^{M}A_{\beta i}\sin(k_ir+\varphi_\beta)}{\left(\sum_{i=1}^{M}\left[A_{\beta i}\cos(k_ir+\varphi_\beta)\right]\right)^2}\right].$$

It is straightforward to show that $\Psi = 0$: From eq. (10),

$$\left[A_\beta(r,z,\omega)\right]_j = \frac{1}{\sqrt{2\pi r k_j}} C_j. \tag{B4}$$

Differentiating with r yields

$$\frac{\partial\ A_\beta(r,z,\omega)\big|_j}{\partial r} = -\frac{A_\beta(r,z,\omega)\big|_j}{2r}. \tag{B5}$$

Hence the numerator of Ψ yields:

$$\frac{1}{2r}\left\{\sum_{i=1}^{M} A_{\beta i}\sin(k_i r+\varphi_\beta)\sum_{i=1}^{M} A_{\beta i}\cos(k_i r+\varphi_\beta) - \sum_{i=1}^{M} A_{\beta i}\cos(k_i r+\varphi_\beta)\sum_{i=1}^{M} A_{\beta i}\sin(k_i r+\varphi_\beta)\right\} = 0.$$

With $\Psi = 0$, eq. (B3) becomes:

$$\frac{\partial\psi_\beta}{\partial r} = \frac{\sum_{i=1}^{M} A_{\beta i}k_i\cos(k_i r+\varphi_\beta)\sum_{i=1}^{M} A_{\beta i}\cos(k_i r+\varphi_\beta) + \sum_{i=1}^{M} A_{\beta i}k_i\sin(k_i r+\varphi_\beta)\sum_{i=1}^{M} A_{\beta i}\sin(k_i r+\varphi_\beta)}{\left(\sum_{i=1}^{M}\left[A_{\beta i}\cos(k_i r+\varphi_\beta)\right]\right)^2 + \left(\sum_{i=1}^{M}\left[A_{\beta i}\sin(k_i r+\varphi_\beta)\right]\right)^2}. \tag{B6}$$

Finally, eq. (B1) becomes

$$\hat{V}_\beta(r,z,\omega) = \omega\frac{\left(\sum_{i=1}^{M}\left[A_{\beta i}\cos(k_i r+\varphi_\beta)\right]\right)^2 + \left(\sum_{i=1}^{M}\left[A_{\beta i}\sin(k_i r+\varphi_\beta)\right]\right)^2}{\sum_{i=1}^{M} A_{\beta i}k_i\cos(k_i r+\varphi_\beta)\sum_{i=1}^{M} A_{\beta i}\cos(k_i r+\varphi_\beta) + \sum_{i=1}^{M} A_{\beta i}k_i\sin(k_i r+\varphi_\beta)\sum_{i=1}^{M} A_{\beta i}\sin(k_i r+\varphi_\beta)}. \tag{B7}$$

As shown in eq. (A5), an alternative representation for the numerator of eq. (B7) holds which is formally given by as a double summation. To obtain eq. (9) it must be shown that:

$$\sum_{i=1}^{M} A_{\beta i}k_i\cos(k_i r+\varphi_\beta)\sum_{i=1}^{M} A_{\beta i}\cos(k_i r+\varphi_\beta) + \sum_{i=1}^{M} A_{\beta i}k_i\sin(k_i r+\varphi_\beta)\sum_{i=1}^{M} A_{\beta i}\sin(k_i r+\varphi_\beta)$$

$$= \frac{1}{2}\sum_{i=1}^{M}\sum_{j=1}^{M}\left[A_{\beta i}A_{\beta j}(k_i+k_j)\cos(r[k_i-k_j])\right]. \tag{B8}$$

Using induction, assuming eq. (B8) is true for $M = n$, it suffices to prove that it is also true for $n+1$:

$$\begin{aligned} S_{n+1} &= \sum_{i=1}^{n+1} A_i k_i\cos(k_i r+\varphi_\beta)\sum_{i=1}^{n+1} A_i\cos(k_i r+\varphi_\beta) + \sum_{i=1}^{n+1} A_i k_i\sin(k_i r+\varphi_\beta)\sum_{i=1}^{n+1} A_i\sin(k_i r+\varphi_\beta) \\ &= \left[\sum_{i=1}^{n} A_i k_i\cos(k_i r+\varphi_\beta) + A_{n+1}k_{n+1}\cos(k_{n+1}r+\varphi_\beta)\right]\left[\sum_{i=1}^{n} A_i k_i\cos(k_i r+\varphi_\beta) + A_{n+1}\cos(k_{n+1}r+\varphi_\beta)\right] \\ &\quad + \left[\sum_{i=1}^{n} A_i k_i\sin(k_i r+\varphi_\beta) + A_{n+1}k_{n+1}\sin(k_{n+1}r+\varphi_\beta)\right]\left[\sum_{i=1}^{n} A_i k_i\cos(k_i+\varphi_\beta) + A_{n+1}\sin(k_{n+1}+\varphi_\beta)\right], \end{aligned} \tag{B9}$$

$$\begin{aligned} S_{n+1} &= (A_{n+1})^2 k_{n+1}\cos^2(k_{n+1}+\varphi_\beta) + A_{n+1}\sum_{i=1}^{n} A_i k_i\cos(k_i r+\varphi_\beta)\cos(k_{n+1}r+\varphi_\beta) + A_{n+1}k_{n+1}\sum_{i=1}^{n} A_i\cos(k_i r+\varphi_\beta)\cos(k_{n+1}r+\varphi_\beta) \\ &\quad + \sum_{i=1}^{n} A_i\cos(k_i r+\varphi_\beta)\sum_{i=1}^{n} A_i k_i\cos(k_i r+\varphi_\beta) + (A_{n+1})^2 k_{n+1}\sin^2(k_{n+1}+\varphi_\beta) + A_{n+1}\sum_{i=1}^{n} A_i k_i\sin(k_i r+\varphi_\beta)\sin(k_{n+1}r+\varphi_\beta) \\ &\quad + A_{n+1}k_{n+1}\sum_{i=1}^{n} A_i\sin(k_i r+\varphi_\beta)\sin(k_{n+1}r+\varphi_\beta) + \sum_{i=1}^{n} A_i\sin(k_i r+\varphi_\beta)\sum_{i=1}^{n} A_i k_i\sin(k_i r+\varphi_\beta). \end{aligned} \tag{B10}$$

By the assumption used in induction:

$$\begin{aligned} S_{n+1} &= A_{n+1}^2 k_{n+1}\cos(k_{n+1}-k_{n+1}) + A_{n+1}\sum_{i=1}^{n} A_i k_i\cos(k_i-k_{n+1}) + A_{n+1}k_{n+1}\sum_{i=1}^{n} A_i\cos(k_i-k_{n+1}) \\ &\quad + \frac{1}{2}\sum_{i=1}^{n}\sum_{j=1}^{n}\left[A_i A_j(k_i+k_j)\cos(r[k_i-k_j])\right]. \end{aligned} \tag{B11}$$

It is remarked that:

$$S'_{n+1} = \sum_{i=1}^{n+1}\sum_{j=1}^{n+1}\left[A_i A_j k_i \cos\left(r[k_i - k_j]\right)\right]$$

$$= \sum_{i=1}^{n+1}\sum_{j=1}^{n}\left[A_i A_j k_i \cos\left(r[k_i - k_j]\right) + A_i A_{n+1} k_i \cos\left(r[k_i - k_{n+1}]\right)\right]$$

$$= \sum_{i=1}^{n}\sum_{j=1}^{n}\left[A_i A_j k_i \cos\left(r[k_i - k_j]\right)\right] + A_{n+1}\sum_{i=1}^{n}\left[A_i k_i \cos\left(r[k_i - k_{n+1}]\right)\right]$$

$$+ A_{n+1}k_{n+1}\sum_{j=1}^{n}\left[A_j \cos\left(r[k_j - k_{n+1}]\right)\right] + A_{n+1}^2 k_{n+1}\cos\left(k_{n+1} - k_{n+1}\right). \tag{B12}$$

Finally:

$$\frac{1}{2}\sum_{i=1}^{n+1}\sum_{j=1}^{n+1}\left[A_i A_j (k_i + k_j)\cos\left(r[k_i - k_j]\right)\right] = \frac{1}{2}\sum_{i=1}^{n}\sum_{j=1}^{n}\left[A_i A_j (k_i + k_j)\cos\left(r[k_i - k_j]\right)\right] + A_{n+1}\sum_{i=1}^{n}\left[A_i k_i \cos\left(r[k_i - k_{n+1}]\right)\right]$$

$$+ A_{n+1}k_{n+1}\sum_{j=1}^{n}\left[A_j \cos\left(r[k_j - k_{n+1}]\right)\right] + A_{n+1}^2 k_{n+1}\cos\left(k_{n+1} - k_{n+1}\right) = S_{n+1}. \tag{B13}$$